Controllable Tuning Various Ratios of ZnO Materials Polar Facets in Dimethylacetamide Media and their Kinetic Photocatalytic Activity

[1, 2]Weiliang Feng, [1, 3]Min Tao and [4]Pei Huang*
[1]*Key Laboratory of Green Chemical Process of Ministry of Education, Wuhan Institute of Technology, Wuhan 430073, China.*
[2]*Key Laboratory of Novel Reactor and Green Chemical Technology of Hubei Province, Wuhan Institute of Technology, Wuhan 430073, China.*
[3] *School of Chemical Engineering and Pharmacy, Wuhan Institute of Technology, Wuhan 430073, China.*
[4] *State Key Laboratory of Materials-Oriented Chemical Engineering, College of Chemistry and Chemical Engineering, Nanjing University of Technology, Nanjing 210009, Jiangsu, PR China.*
phuang1965@126.com*

(Received on 20th February 2017, accepted in revised form4th December 2017)

Summary: Controllable ZnO materials with different morphologies were synthesized via a simple solvothermal method in dimethylacetamide (DMAc) media. The significance of the synthetic strategy is the generation of exotic structures without using any templates/structure directing agents and successful realization of different morphologies. Detailed investigation revealed that the size and shape of ZnO materials can be conveniently tailored by systematically exercising control on the choice of contents of DMAc. The optical properties of the as-prepared ZnO materials were investigated by room temperature photoluminescence. Photodegradation of phenol was used as a model reaction to test the photocatalytic activity of the ZnO products. The morphology-dependent photocatalytic performances in the degradation of phenol under UV light illumination were observed, in which the ZnO spherical nanoparticles exhibit the highest activity. The kinetic behavior of a photocatalytic reaction can be described by a pseudo-first order model. The efficiency of degradation of the as-prepared ZnO spherical nanoparticles structures was more than twice times faster than that of using ZnO rods under the UV light irradiation. Moreover, the as-prepared products exhibited high photostability, and degradation efficiency could be slightly decreased even after being used three cycles. The possible mechanism for the difference photocatalytic activity of the as-prepared ZnO structures was also discussed.

Keywords: ZnO Crystals; Solvothermal process; DMAc solvent; Optical properties; Photocatalytic activity.

Introduction

ZnO, an II-VI semiconductor with noncentrosymmetric wurtzite crystal structure, a direct band gap of 3.37 eV, and a large excitation binding energy of 60 meV, has been extensively investigated because of its potential applications in piezoelectric devices [1], transistors [2], photodiodes [3], and photocatalysis [4]. Among these applications of ZnO, the photocatalysis is the most important one for environmental protection. In the field of photocatalysis, ZnO is usually believed to be an alternative photocatalyst material to TiO_2, since they have similar band gaps and similar photocatalytic mechanisms [5]. Many works reported that ZnO shows even better photocatalytic activity than TiO_2 [6].

Due to the fact that a photocatalytic reaction occurs at the interface between catalyst and organic pollutants, the photocatalytic performance of ZnO is strongly dependent on the growth manner of the crystal, and it has been demonstrated that the morphology control could result in optimization of the photocatalytic activity of ZnO photocatalyst [7]. The conclusion has been attributed to the fact that the catalytic performance of nanocrystals is determined either by the composition in terms of the atomic structure or by the morphologies that effect surface atomic arrangements and coordination [8]. Therefore, control of the size, shape, and preferred orientation of ZnO nanostructures to tailor its chemical and physical properties for optimum reactivity and selectivity is very important. At present, ZnO materials with different architectures, such as rods, tubes, plates, porous hollow microspheres, and flower-like hierarchical micro/nanoarchitecture, were fabricated by chemical vapor deposition [9], thermal evaporation [10], and wet-chemical routes including sol-gel processes [11] and solvothermal (hydrothermal) methods [12]. Apart from synthetic methods, the morphologies and photocatalytic performance of ZnO nanostructures are also dramatically affected by the use of soft templates [13], surfactants [14], growth modifiers [15], and capping agents [16]. These findings potentially open an

*To whom all correspondence should be addressed.

avenue for the preparation of efficient ZnO photocatalyst for photocatalytic degradation of organic pollutants. However, some of these synthetic methods involve complex procedures, sophisticated equipments, rigorous experimental conditions or long processing time [17-19]. In addition, although several papers have reported the preparation of ZnO samples and their photocatalytic application, comparison studies on the correlation between the morphology and photocatalytic property have seldom been reported in detail.

To investigate the effect of the morphologies of ZnO on photocatalytic properties, it is worthy of developing a simple and cost-effective method to prepare ZnO photocatalyst with different morphologies. In the present work, ZnO materials with a range of different morphologies were prepared by the solvothermal method in dimethylacetamide (DMAc) media. DMAc was used not only as a solvent but also as a base source for the direct growth of ZnO crystals. ZnO materials with different crystallite and particle sizes could be prepared by controlling DMAc contents. The degradation of phenol under the UV light irradiation is used as a model system to showcase the photocatalytic activity. ZnO materials with different crystal growth habits showed significant differences in catalytic performance for phenol photodegradation. The photocatalytic activity mechanism for the formation of ZnO materials with a range of different morphologies was also discussed.

Experimental

Synthesis of ZnO

The typical experiment procedure was as follows: 20 mM of zinc acetate was dissolved in solvent with different volume ratios (DMAc:H_2O) of 1:4, 2:3, 3:2, 4:1, and pure DMAc. The growth process was carried out at 95 °C for 3 h. After the expected time the samples were cooled down to room temperature. The formed white precipitates were separated by centrifugation and washed thoroughly with deionized water. The washing steps were repeated three times to remove the DMAc organic solvent. Subsequently, the white precipitates were dried in air at 80 ºC overnight. The different reaction conditions and the products were summarized in Table-1.

Structure characterization

The crystalline structures of the products were recorded by X-ray powder diffraction (D8 Advance, Bruker) with a Cu Kα (λ=0.15406 nm) radiation source at 40 kV and 30 mA. The morphologies of the as-synthesized samples were observed using scanning electron microscopy (S-4800, Hitachi). X-ray photoelectron spectroscopy (XPS) were performed using a Vacuum Generator Mutilab 2000 spectrometer with an excitation source of Al Ka=1486.6 eV. Photoluminescence (PL) measurements were carried out on a Varian Cary Eclipse spectrophotometer by a 325 nm excitation from Xe lamp at room temperature. A 200 kV transmission electron microscope (JEM-2100, JEOL) was utilized to study the microstructures of the samples. The total organic C was measured using an automated total organic C analyzer (TOC-2000, Shanghai Metash Instruments Co.,LTD., China). The surface area was determined with the Brunauer-Emmett-Teller (BET) method using N_2 adsorption (ASAP-2460, Micromeritics).

Table-1: The different reaction conditions and the products.

Sample	solvent	ZnO products	BET surf.area (m^2/g)
A	DMAc:H_2O=1:4	Fig. 2a	11.054
b	DMAc:H_2O=2:3	Fig. 2b	9.316
c	DMAc:H_2O=3:2	Fig. 2c	2.284
d	DMAc:H_2O=4:1	Fig. 2d	1.699
e	pure DMAc	Fig. 2e	1.448

Photocatalytic degradation of phenol

Phenol was employed as a representative organic pollutant to evaluate the photocatalytic activity of ZnO with different morphologies for its degradation. Approximately 50 mg ZnO powder products were added into 100 mL phenol solution. The solution was then exposed to light from a 30W UV lamp (Haimen Kylin-Bell Lab Instrument Factory, ZF-1) with wavelength centered at 365 nm. The above mixture solution was irradiated in a photochemical chamber under continuous stirring. Before irradiation, the solution was stirred for 30 min in the dark to reach an adsorption-desorption equilibrium between the photocatalyst and phenol. At certain time intervals, 3 mL solution was drawn out each time and centrifuged at 5000 rpm for 5 min to get clear liquid. The quantitative determination of phenol was performed by measuring its intensity of the absorption peak with a UV-vis spectrophotometer (Shanghai Metash Instrument Factory, UV-6000). The concentration of phenol was determined by monitoring the changes in the main absorbance centered at 269.7 nm.

Results and Discussion

Structure and Morphology

The XRD patterns obtained from the samples obtained with different volume ratios of DMAc to H_2O

are similar, and the typical patterns were shown in the Fig.1. All diffraction peaks can be attributed to hexagonal wurtzite ZnO (JCPDS no. 36-1451). No diffraction peaks from other impurities were observed in the XRD patterns. The sharp and intensive diffraction peaks indicate good crystallinity of ZnO products can be produced via a simple and comparatively low-temperature heat-treatment process.

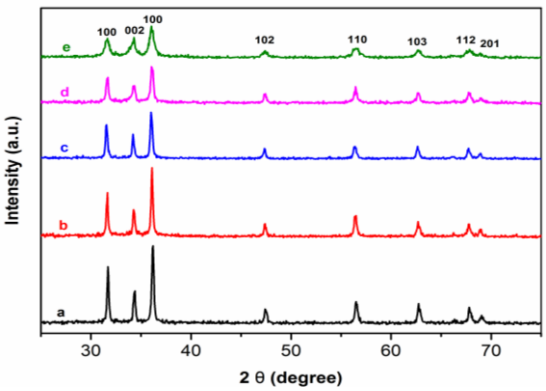

Fig. 1: XRD patterns of the ZnO products fabricated at different volume ratios of DMAc:H_2O. (a) 1:4, (b) 2:3, (c) 3:2, (d) 4:1 and (e) pure DMAc.

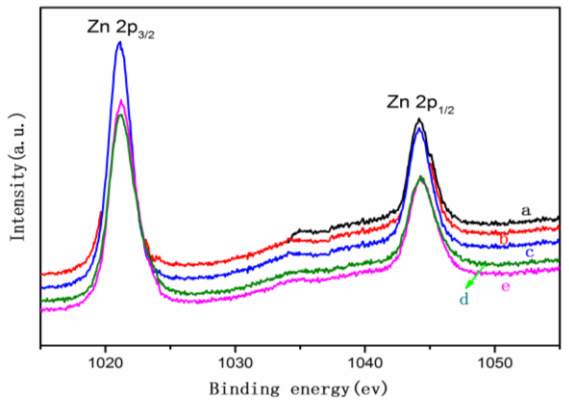

Fig. 2: XPS patterns of the ZnO samples fabricated at different volume ratios of DMAc:H_2O. (a) 1:4, (b) 2:3, (c) 3:2, (d) 4:1, (e) pure DMAc.

The XPS spectrums of Fig. 2 can provide further significant information about the quality and composition of crystals prepared at different volume ratios of DMAc to H_2O. The binding energies obtained in the XPS analysis were corrected for specimen charging by referencing the C 1s to 285.0 eV. In all the cases, from Fig. 2a-e, two strong peaks centered on 1021.1 and 1044.2 eV, which are in agreement with the binding energies of Zn $2p_{3/2}$ and Zn $2p_{1/2}$, respectively. These results indicated that the chemical valence of Zn at the surface of ZnO microstructures is +2 oxidation states [20].

Further structural characterization of spherical nanoparticles with TEM was shown in Fig. 3. Fig.3 showed that the product had a typical spherical-like structure, and the nanoparticles with a diameter of 600 nm were found taking together.

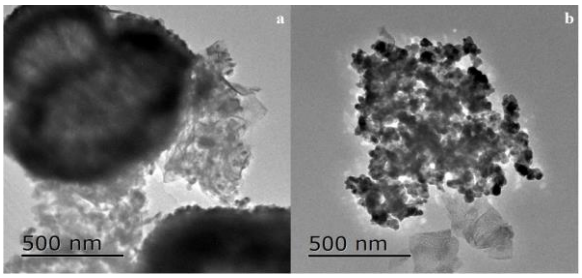

Fig. 3: TEM images of ZnO with spherical-like structure.

The morphologies of the products synthesized for different volume ratios of DMAc to H_2O were shown in Fig. 4(a-e). It can be clearly observed that the evolution of morphology and size of ZnO structures depend on the DMAc content in the solvent. A low-magnification view of the products synthesized in a solution of 20% (v/v) DMAc shown in Fig. 4a demonstrated that the product are composed of micro-rods structures with an average length of 4 μm. With increasing the content of DMAc to 40% (v/v), the morphology of ZnO crystals remain unchanged (Fig. 4b). However, it can be seen that the average length of the ZnO rods is smaller than the average length of the rods shown in Fig. 4a. There is a distinct change in the planar view, from ZnO rods to dumbbell, when the content of DMAc was increased from 40% (v/v) to 60% (v/v). The general SEM image (Fig. 4c) of ZnO samples revealed that the samples were uniform, dumbbell-like structured microcrystals. The surface of this kind of ZnO microcrystal is smooth and its length is up to 0.8 μm. When the content of DMAc was further increased to 80% (v/v), almost all of the final products are composed of quasi-spherical nanoparticles structures (Fig. 4d). The diameters of the nanoparticles varied a great deal, from 200 to 700 nm. As shown in Fig. 4e, the ZnO samples formed in a pure DMAc solvent does not reveal significant difference in the morphology from that of the ZnO nanoparticles shown in Fig. 4d. The product is composed of uniform spherical nanoparticles structures with an average diameter of 600 nm. These observations indicated that the dramatic influence of content of DMAc solvent on the morphology and size of the products.

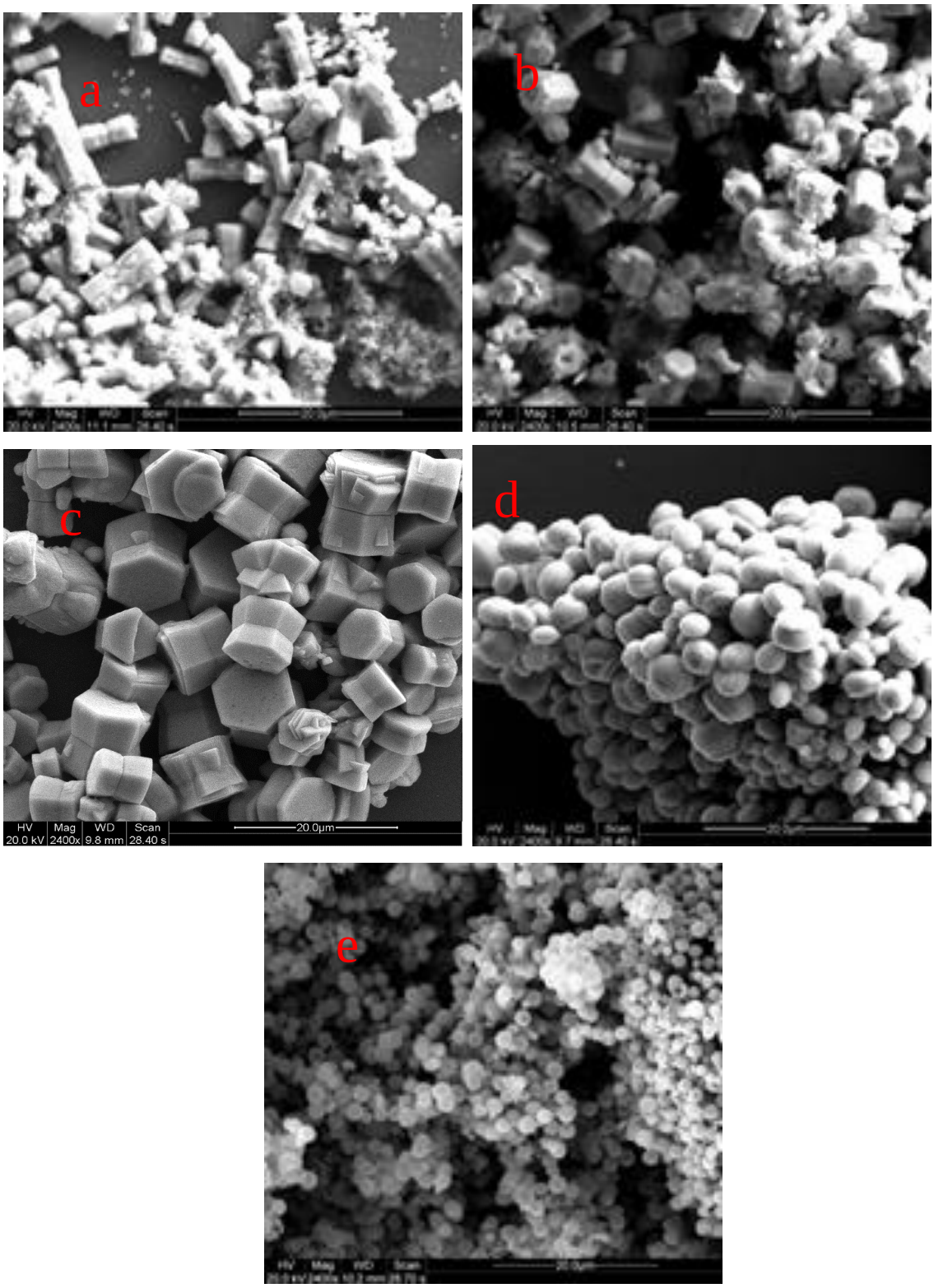

Fig. 4: SEM images of the ZnO products fabricated at different volume ratios of DMAc:H_2O. (a) 1:4, (b) 2:3, (c) 3:2, (d) 4:1 and (e) pure DMAc.

Optical Properties

Raman spectroscopy was carried out to study the vibrational properties of as-grown ZnO crystals at different volume ratios of DMAc to H_2O. Fig. 5 presented the Raman spectrums of these samples at the range of 300-650 cm^{-1}. The dominant feature around 438 cm^{-1} is due to E2 (high) mode, which is a typical Raman peak of bulk ZnO crystal [21]. It is found that the E2 (high) mode becomes stronger when the DMAc content decreases, which may mean improved crystallinity of the as-prepared ZnO crystals. The peaks at 382 and 411 cm^{-1} correspond to A1 (TO) and E1 (TO) phonons of ZnO crystal, respectively [22]. The peak located at 333 cm^{-1} may be attributed to a multiphonon scattering process (E2H-E2L)[23, 24].

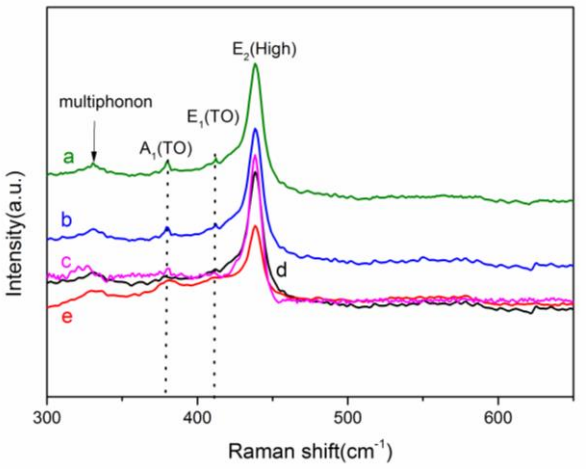

Fig. 5: Raman spectrums of the ZnO samples fabricated at different volume ratios of DMAc:H_2O. (a) 1:4, (b) 2:3, (c) 3:2, (d) 4:1 and (e) pure DMAc.

The optical property of ZnO strongly depends on its structural property, such as crystallinity, surface state and defects [25]. Therefore, structural property of ZnO crystals is further characterized by PL spectroscopy as shown in Fig. 6. The typical room-temperature photoluminescence (PL) spectrums of as-grown ZnO samples at different volume ratios of DMAc to H_2O. The PL spectrums showed similar PL features, in which two obvious luminescence bands were observed, including a strong UV, a weak blue emission bands centered at about 380 nm and 440 nm, respectively. The strong UV emission band results from near-band-gap emission, namely the recombination of free excitons through an exciton-exciton collision process [26]. The weak blue emission peak can be due to the existence of intrinsic defects in the ZnO [27]. Furthermore, the strong UV emission band and weak visible emission band indicate that the as-synthesized ZnO samples have high crystal quality and low concentration of defect.

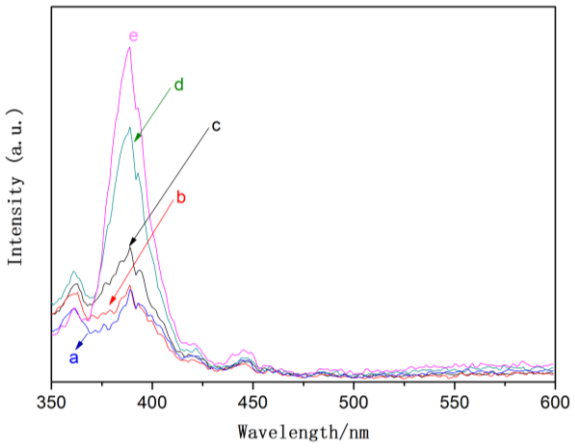

Fig. 6: Room temperature PL spectrums of the ZnO products fabricated at different volume ratios of DMAc:H_2O. (a) pure DMAc, (b) 4:1, (c) 3:2, (d) 2:3 and (e) 1:4.

Photocatalytic activity

As an advanced oxidation processes, semiconductor photocatalysis has been extensively studied for the degradation of toxic pollutants in the environment. Industrial organic pollutants have caused significant environmental problems globally. The degradation and mineralization of organic pollutants using nanostructured semiconductor has attracted great interest in recent years.

To verify the photocatalytic activity of the semiconductor products obtained in the study, the products were tested for organic pollutant degradation process under UV light illumination. In the case, organic pollutant phenol was selected as the model to investigate the photocatalytic activities of the products. The photocatalytic activities of the as-synthesized products are shown in Fig. 7. C_0 and C are the initial concentration after the equilibrium adsorption and the reaction concentration of phenol, respectively. The characteristic absorption of the phenol seen at 269.7 nm was selected for monitoring the adsorption and photocatalytic degradation process.

In absence of catalyst, only a minimal decrease in the concentration of phenol was detected (Fig. 7f). The photocatalytic effect and degradation of phenol were obvious under UV light irradiation in the presence of synthesized ZnO, and the products exhibit different photoactivities depending on the morphology. As seen in Fig. 7, phenol aqueous solution can be obviously degradation by all of the as-synthesized products. The ZnO rods exhibited much lower photocatalytic activity compared with other morphologies of ZnO. The degradation efficiencies for 7e and 7d are only 44.3% and 48.8% within 180 min, respectively. It can be seen that the photocatalytic activity of the ZnO with dumbbell-like structures (7c) was higher that of the ZnO rods for the photodegradation of phenol under UV light irradiation. Interestingly, it was observed that the ZnO with spherical nanoparticles structures displayed the best photocatalytic efficiency (70.7%) amongst the as-synthesized samples in the present study.

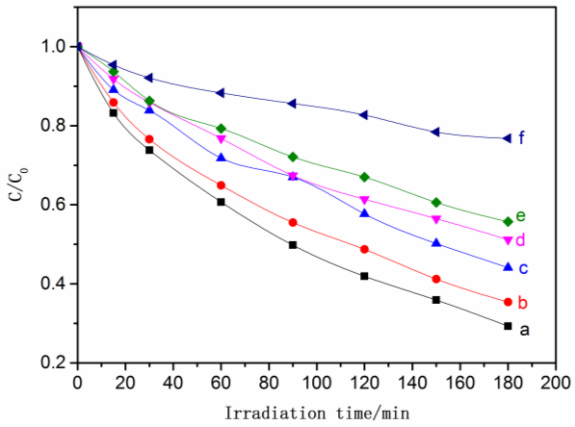

Fig. 7: Photodegradation of phenol using the as-synthesized ZnO products with different morphologies under UV light irradiation. (a) pure DMAc, (b) DMAc:H_2O=4:1, (c) DMAc:H_2O=3:2, (d) DMAc:H_2O=2:3, (e) DMAc:H_2O=1:4 and (f) without catalyst.

For a better understanding of the photocatalytic activities of the as-synthesized products, the kinetic analysis of phenol degradation was also discussed in terms of Langmuir-Hinshelwood (L-H) model [28]. This model has been used successfully to describe the kinetics of the solid-liquid system in heterogeneous photocatalysis qualitatively [29]. In this model, the reaction rate r can be expressed as

$$r = \frac{k_1 k_2 C}{1 + k_2} \qquad (1)$$

where k1 is the apparent rate constant, k2 is the adsorption constant, and C is the reactant concentration. The photocatalytic process was carried out in batch reactor:

$$-V\frac{dC}{dt} = \frac{mAk_1C}{1 + k_2C} \qquad (2)$$

where V is the liquid volume and A is the number of adsorption sites per gram of catalyst. Integration the left-hand side of equation 2 from t=0 to t=i and the right-hand side from initial concentration C0 to final concentration Ci (at t=i):

$$\frac{\ln(C_0/C)}{C_0 - C} = -k_2 + \frac{mAk_1k_2t}{V(C_0 - C)} \qquad (3)$$

As shown in Fig. 8, the photodegradation process undergoes pseudo-first-order kinetics, thus the value of the rate constant equals the corresponding slope of the linear fitting line. Fig. 8 showed the pseudo-first-order rate constants (k) of the products decreasing in the order: a>b>c>d>e. The calculated k for the ZnO with spherical nanoparticles is 2.83×10-3 min^{-1}, which is 2.07 times higher than that of the ZnO with rods (1.37×10-3 min^{-1}). Obviously, the ZnO spherical nanoparticles exhibited the hightest rate constant for photodegradation of phenol under UV light irradiation. The corresponding pseudo- first-order rate constants were displayed in Table-2.

Table-2: Apparent first order kinetic rate for the degradation of phenol under UV light irradiation. (a) pure DMAc, (b) DMAc:H_2O=4:1, (c) DMAc:H_2O=3:2, (d) DMAc:H_2O=2:3 and (e) DMAc:H_2O=1:4.

sample	k(min^{-1})	R^2
a	0.00283	0.9903
b	0.00239	0.9895
c	0.00191	0.9929
d	0.00157	0.9884
e	0.00137	0.9919

The total organic carbon (TOC) was used to evaluate the degree of degradation or mineralization

of phenol in this study (Fig.9). It can be seen that partial the organic matter was mineralized. However, the TOC removal efficiency is not high. The reason has been attributed to the fact that partial phenol may be degraded or converted other organic matter. Further investigations are thus required to uncover this phenomenon, and this is the next step in our future studies.

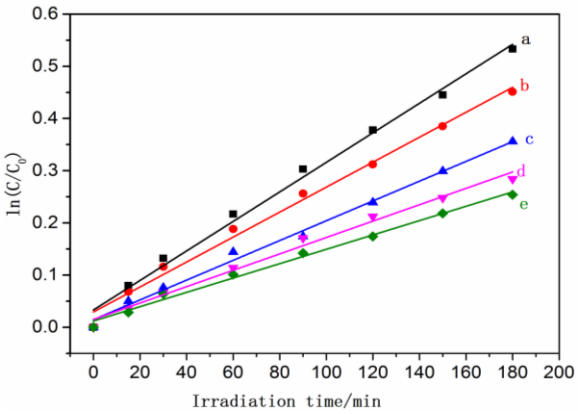

Fig. 8: The kinetic curves of the as-synthesized ZnO products with different morphologies for phenol degradation. (a) pure DMAc, (b) DMAc:H2O=4:1, (c) DMAc:H2O=3:2, (d) DMAc:H2O=2:3 and (e) DMAc:H2O=1:4.

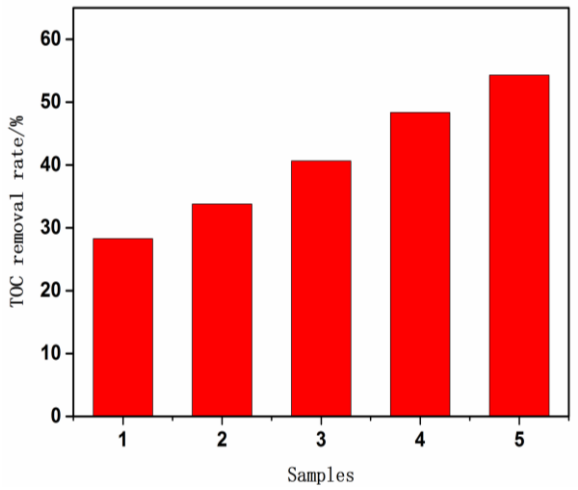

Fig. 9: TOC removal rate of of the as-synthesized ZnO products with different morphologies for phenol degradation. (1) DMAc:H2O=1:4, (2) DMAc:H2O=2:3, (3) DMAc:H2O=3:2, (4) DMAc:H2O=4:1 and (5) pure DMAc.

Photostability

To investigate the stability of photocatalytic performance under UV light irradiation, the products with different morphologies were used to degrade phenol in three repeated cycles, and the results were shown in Fig. 10. After each cycle which lasts for 180 min, the photocatalyst was separated from the suspension by filtration, washed with deionized water, dried and weighed for a new cycle. Moreover, it can be found that the mass loss percent of photocatalyst during each cycle is low than 5 wt.%, which means the recovery efficiency of ZnO is above 95% for each cycle.

From the Fig. 10, it can be seen that the ZnO with different morphologies exhibited excellent photochemical stability. The photocatalytic efficiency reduced only by 3.07%-3.4% after three cycles. It was noteworthy that the photocatalytic performance of the ZnO spherical nanoparticls exhibited effective photostability under UV light irradiation. Furthermore, because of the high photocatalytic activity of ZnO nanoparticles structures and excellent photochemical stability, it is still able to achieve a 70% degradation efficiency of phenol in the first three cycles.

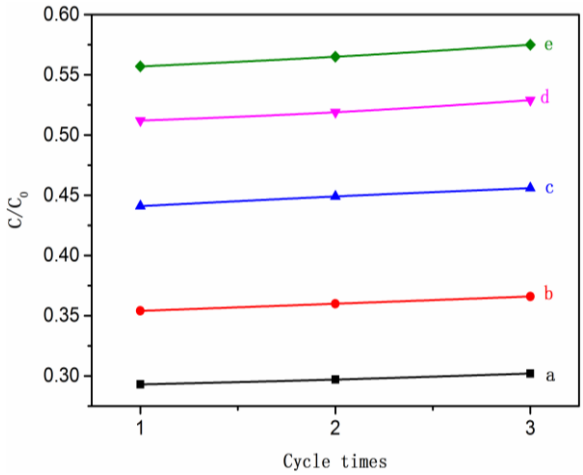

Fig. 10: Three photocatalytic degradation cycles of phenol using the as-synthesized ZnO products with different morphologies under UV light irradiation. (a) pure DMAc, (b) DMAc:H2O=4:1, (c) DMAc:H2O=3:2, (d) DMAc:H2O=2:3 and (e) DMAc:H2O=1:4.

Photocatalytic Mechanism

The photocatalytic mechanism contains three process: 1. light absorption, 2. charge separation and 3. photocatalytic reaction on the semiconductor surfaces [30]. Upon irradiation of ZnO structures by UV light, the electron in valance band of ZnO structures were excited into the conduction band. The holes in the valance band will react with water and generate OH· radicals and electrons in the conduction band will produce superoxide anion radical (O·) [31-33]. The successive formation of these radicals leads the efficient photocatalytic degradation of phenol (Fig. 11).

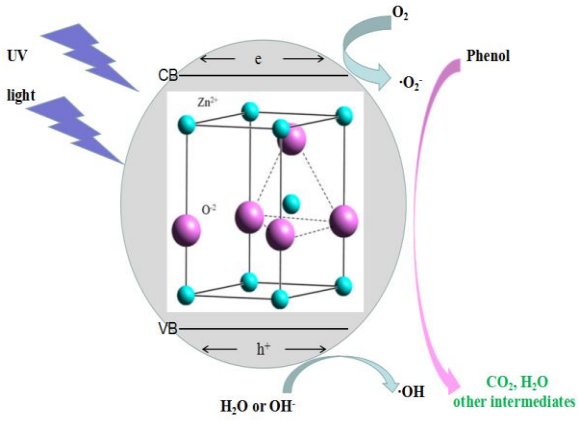

Fig. 11: Schematic representation of the possible mechanism behind the photocatalytic activity of as-grown ZnO structures upon degradation of phenol induced by UV light irradiation.

In general, the photocatalytic activity of an oxide semiconductor is closely related to the particle sizes, morphologies, and surface properties [34, 35]. Clearly, ZnO products with different morphologies reveal significant difference at photodegradation in the present study. To demonstrate the morphology induced superior photocatalytic performances of ZnO with spherical shapes over the other morphologies synthesized, photocatalytic activity of ZnO rods was also studied. It is evident from our findings that these rod-shaped products with the highest aspect ratio show the poorest photocatalytic activity. The schematic illustration (Fig. 12) represented the trend of increasing photocatalytic activity as observed for the synthesized samples studied.

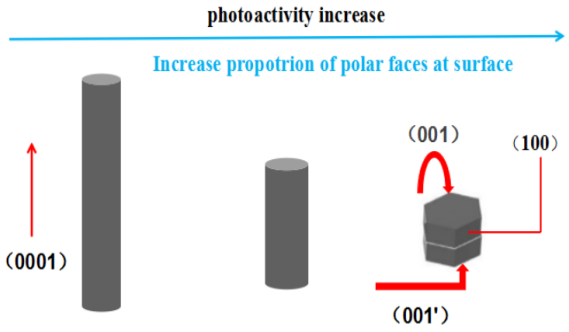

Fig. 12: A schematic illustration representing the correlation between polar facets and photocatalytic activity trends for the ZnO structures.

A significant difference between products with different morphologies has been attributed to the fact that the proportion of different crystal facets present on the surface of the products. The surface of a c-axis-aligned rod mostly consists of nonpolar faces parallel to the rod axis, whereas the dominant surfaces exposed on a dumbbell-like structures are the polar (001) Zn face and the (001') O face, as illustrated in Fig. 12. The data clearly implied that exposure of a greater proportion of polar faces leads to greater photocatalytic activity. The high activity of the (001) Zn face could be attributed to the (001) face of ZnO, the face with the intrinsically highest energy among all the faces [36]. The OH- ions could preferentially adsorb onto this face because of its positive charge [37]. This would lead to a greater rate of production of OH· radicals, and hence degradation of the organic solution, during the photocatalysis. Zeng et al. have hydrothermally synthesized single crystalline ZnO nanodisks and nanowires and have shown that ZnO nanodisks with a high population of (001) facets show better catalytic activity for photodegradation of rhodamine B dye as compared to ZnO nanowires [38]. Zhai et al. synthesized ZnO nanodisks, consisting of nanocrystals by a simple chemical hydrolysis method, which exhibited high photocatalytic activity towards degradation of methyl orange [39]. Considering the evidence described above, it may be concluded that dumbbell-like structured have more numbers of the active sites as compared to other rods morphologies. Hence, the ZnO dumbbell-like have a higher photodegradation efficiency than the ZnO rods in the present study.

Interestingly, the ZnO nanoparticles showed the best photocatalytic efficiency in our work. There was no correlation between the surface areas and the

catalytic activity data for our materials demonstrating that there are other more important factors that govern activity. Several studies reported that higher surface area of catalysts did not result in higher catalytic performance [40]. When the photocatalyst reached the nanoscale size, the chance of recombining electron–hole pairs decreases because of the fast arrival of electrons at the reaction sites located on the surface of the catalyst [41]. The smaller size of the spherical nanoparticles with an average diameter of 600 nm, which is substantially smaller than that of other morphologies (4 μm). With all the mentioned before, it might be concluded that the superior photoactivity of the spherical nanoparticles can be attributed to their exotic structural features with predominantly exposed active polar facets, which can increase the number of active sites and promote the separation efficiency of the electron–hole pairs in the photocatalytic reactions. Additionaly, the spherical nanoparticles has a relatively lower crystallinity and more defects. Defects usually are located on the surface when semiconductor materials are fabricated with solution method. The phenol would be photocatalyzed because more naked Zn atoms on the crystal defects bind O atoms of phenol molecules. The defects in crystals especially on the surface can serve as active sites which play a major role for the catalytic activity [42]. So, crystallinity is an important factor that is responsible for this catalytic activity. Further experiments are therefore needed in order to address the origin of the high photocatalytic activity of the spherical nanoparticles reported in this note.

Conclusion

Controllable ZnO architectures with different morphologies were synthesized via a simple solvothermal method in dimethylacetamide (DMAc) media. Detailed investigation revealed that the size and shape of ZnO microstructures can be conveniently tailored by systematically exercising control on the choice of content of DMAc. Photodegradation of phenol was used as a model reaction to test the photocatalytic activity of the ZnO products. The morphology-dependent photocatalytic performances in the degradation of phenol under UV light illumination were observed, in which the ZnO spherical nanoparticles exhibit the highest activity. The efficiency of degradation of the as-prepared ZnO nanoparticles structures was more than twice times faster than that of using ZnO rods under the UV light irradiation. Moreover, the as-prepared products exhibited high photostability, and degradation efficiency could be slightly decreased even after being used three cycles. The possible mechanism for the difference photocatalytic activity of the as-prepared ZnO structures was also discussed.

Acknowledgements

This work was supported by The Guiding Program of Department of Education of Hubei (B2016055).

References

1. P. L. Wang, Y. M. Fu, B. W. Yu, Y. Y. Zhao, L. L. Xing, X. Y. Xue, Realizing room-temperature self-powered ethanol sensing of ZnO nanowire arrays by combining their piezoelectric, photoelectric and gas sensing characteristics, *J. Mater. Chem*. A, **3**, 3529 (2015).
2. E. Bandiello, M. Sessolo, H. J. Bolink, Aqueous electrolyte-gated ZnO transistors for environmental and biological sensing, *J. Mater. Chem*. C, **2**, 10277 (2014).
3. M. Tyagi, M. Tomar, V. Gupta, Fabrication of an efficient GLAD-assisted p-NiO nanorod/n-ZnO thin film heterojunction UV photodiode, *J. Mater. Chem*. C, 2, 2387 (2014).
4. Y. Q. Sun, Y. G. Sun, T. Zhang, G. Z. Chen, F. S. Zhang, D. L. Liu, W. P. Cai, Y. Li, X. F. Yang, C. C. Li, Complete Au@ZnO core–shell nanoparticles with enhanced plasmonic absorption enabling significantly improved photocatalysis, *Nanoscale*, **8**, 10774 (2016).
5. F. H. Ko, W. J. Lo, Y. C. Chang, J. Y. Guo, C. M. Chen, ZnO nanowires coated stainless steel meshes as hierarchical photocatalysts for catalytic photodegradation of four kinds of organic pollutants, *J. Alloy. Compd*., **678**, 137 (2016).
6. W. He, H. K. Kim, W. G. Wamer, D. Melka, J. H. Callahan, J. J. Yin, Photogenerated charge carriers and reactive oxygen species in ZnO/Au hybrid nanostructures with enhanced photocatalytic and antibacterial activity, *J. Am. Chem. Soc*., **136**, 750 (2014).
7. J. Becker, K. R. Raghupathi, J. S. Pierre, D. Zhao, R. T. Koodali, Tuning of the crystallite and particle sizes of ZnO nanocrystalline materials in solvothermal synthesis and their photocatalytic activity for dye degradation, *J. Phys. Chem*. C, **115**, 13844 (2011).
8. R. Boppella, K. Anjaneyulu, P. Basak, S. V. Manorama, Facile synthesis of face oriented ZnO

crystals: tunable polar facets and shape induced enhanced photocatalytic performance, *J. Phys. Chem*. C, **117**, 4597 (2013).

9. Z. H. Li, E. S. Cho, J. K. Sang, Mg-doped ZnO thin films deposited by the atomic layer chemical vapor deposition for the buffer layer of CIGS solar cell, *Appl. Surf. Sci*., **314**, 97 (2014).
10. M. Tsegaa, D. H. Kuob, F. B. Dejenea, Growth and green defect emission of ZnPbO nanorods by a catalyst-assisted thermal evaporation-oxidation method, *J. Cryst. Growth*, **415**, 106 (2015) .
11. L. Y. Zhang, L. W. Yin, C. X. Wang, N. Lun, Y. X. Qi. Sol - Gel growth of hexagonal faceted ZnO prism quantum dots with polar surfaces for enhanced photocatalytic activity, *ACS Appl. Mater. Interfaces*, **2**, 1769 (2010).
12. W. L. Feng, P. Huang, B. C. Wang, C. W. Wang, W. G. Wang, T. L. Wang, S. F. Chen, R. L. Lv, Y. H. Qin, J. Y. Ma, Solvothermal synthesis of ZnO with different morphologies in dimethylacetamide media, *Ceram. Int.*, **42**, 2250 (2016).
13. Y. Xie, B. Cai, D. Q. Yu, W. J. Shan, W. H. Zhang, Template-guided growth of well-aligned ZnO nanocone arrays on FTO substrate, *J. Cryst. Growth*, **346**, 64 (2012).
14. M. T. Fereidooni, S. Azizian, S. Wettig, Synergistic behaviour of ZnO nanoparticles and gemini surfactants on the dynamic and equilibrium oil/water interfacial tension, *Phys. Chem. Chem. Phys*., **17**, 7122 (2015).
15. Y. Peng, A. W. Xu, B. Deng, M. Antonietti, H. Cölfen, Polymer-controlled crystallization of zinc oxide hexagonal nanorings and disks, *J. Phys. Chem.* B, **110**, 2988 (2006).
16. R. Javed, M. Usman, S. Tabassum, M. Zia, Effect of capping agents: Structural, optical and biological properties of ZnO nanoparticles, *Appl. Surf. Sci*., **386**, 319 (2016).
17. T. Morita, S. Ueno, T. Tokunaga, E. Hosono, Y. Oaki, H. Imai, H. Matsuda, H. Zhou, M. Hagiwara, S. Fujihara, Fabrication of transparent ZnO thick film with unusual orientation by the chemical bath deposition, *Cryst. Growth Des.*, **15**, 3150 (2015).
18. S. W. Bian, I. A. Mudunkotuwa, T. Rupasinghe, V. H. Grassian, Aggregation and dissolution of 4 nm ZnO nanoparticles in aqueous environments: influence of pH, ionic strength, size, and adsorption of humic acid, *Langmuir*, **27**, 6059 (2011).
19. H. Wagata, N. Ohashi, K. I. Katsumata, H. Segawa, Y. Wada, H. Yoshikawa, S. Ueda, K. Okada, N. Matsushita, An aqueous solution process and subsequent UV treatment for highly transparent conductive ZnO films, *J. Mater. Chem*., **22**, 20706 (2012).
20. A. Moulahi, F. Sediri, ZnO nanoswords and nanopills: hydrothermal synthesis, characterization and optical properties, *Ceram. Int*., **40**, 943 (2014).
21. A. Phuruangrat, O. Yayapao, T. Thongtem, S. Thongtem, Preparation, characterization and photocatalytic properties of Ho doped ZnO nanos-tructures synthesized by sonochemical method, *Superlattices Microstruct*., **67**, 118 (2014).
22. Q. Yu, C. Yu, H. Yang, W. Fu, L. Chang, J. Xu, R. Wei, H. Li, H. Zhu, M. Li, G. Zou, G. Wang, C. Shao, Y. Liu, Growth of dumbbell-like ZnO microcrystals under mild conditions and their photoluminescence properties, *Inorg. Chem*., **46**, 6204 (2007).
23. J. H. Yang, J. H. Zheng, H. J. Zhai, L. L. Yang, Low temperature hydrothermal growth and optical properties of ZnO nanorods, *Cryst. Res. Technol*., **44**, 87 (2009).
24. D. Polsongkram, P. Chamninok, S. Pukird, L. Chow, O. Lupanb, G. Chai, H. Khallaf, S. Park, A. Schulte, Effect of synthesis conditions on the growth of ZnO nanorods via hydrothermal method, *Physica* B, **403**, 3713 (2008).
25. P. Rai, W. K. Kwak, Y. T. Yu, Solvothermal synthesis of ZnO nanostructures and their morphology-dependent gas-sensing properties, *ACS Appl. Mater. Interfaces*, **5**, 3026 (2013).
26. Y. H. Ko, M. S. Kim, W. Park, J. S. Yu, Well-integrated ZnO nanorod arrays on conductive textiles by electrochemical synthesis and their physical properties, *Nanoscale Res. Lett.*, **8**, 1 (2013).
27. E. De la Rosa, S. Sepúlveda-Guzman, B. Reeja-Jayan, A. Torres, P. Salas, N. Elizondo, M. Jose Yacaman, Controlling the growth and luminescence properties of well-Faceted ZnO nanorods, *J. Phys. Chem.* C, **111**, 8489 (2007).
28. T. Lo´pez, J. Herna´ndez-Ventura, R. Go´mez, F. Tzompantzi, E. Sa´nchez, X. Bokhimi, A. García, Photodecomposition of 2,4-dinitroaniline on Li/TiO_2 and Rb/TiO_2 nanocrystallite sol–gel derived catalysts, *J. Mol. Catal*. A, **167**, 101 (2001).
29. M. D. L. R. Peralta, U. Pal, R. S. Zeferino, Photoluminescence (PL) quenching and enhanced photocatalytic activity of Au-decorated ZnO nanorods fabricated through

microwave-assisted chemical synthesis, *ACS Appl. Mater. Interfaces*, **4**, 4807 (2012).

30. M. Toubane, R. Tala-Ighil, F. Bensouici, M. Bououdina, W. Cai, S. Liu, M. Souier, A. Iratni, Structural, optical and photocatalytic properties of ZnO nanorods: Effect of aging time and number of layers, *Ceram. Int*., **42**, 9673 (2016).
31. S. S. Patil, M. G. Mali, M. S. Tamboli, D. R. Patil, M. V. Kulkarni, H. Yoon, H. Kim, S. S. Al-Deyabd, S. S. Yoon, S. S. Kolekar, B. B. Kale, Green approach for hierarchical nanostructured Ag-ZnO and their photocatalytic performance under sunlight, *Catal. Today*, **260**, 126 (2016).
32. A. Ghosh, P. Guha, A. K. Samantara, B. K. Jena, R. Bar, S. Ray, P. V. Satyam, Simple growth of faceted Au-ZnO hetero-nanostructures on silicon substrates (nanowires and triangular nano flakes): a shape and defect driven enhanced photocatalytic performance under visible light, *ACS Appl. Mater. Interfaces*, **7**, 9486 (2015).
33. Z. X. Pei, L. Y. Ding, M. L. Lu, Z. H. Fan, S. X. Weng, J. Hu, P. Liu, Synergistic effect in polyaniline-hybrid defective ZnO with enhanced photocatalytic activity and stability, *J. Phys. Chem. C,* **118**, 9570 (2014).
34. N. Huang, J. X. Shu, Z. H. Wang, M. Chen, C. G. Ren, W. Zhang, One-step pyrolytic synthesis of ZnO nanorods with enhanced photocatalytic activity and high photostability under visible light and UV light irradiation, *J. Alloy. Compd*., **648**, 919 (2015).
35. J. H. Lang, J. Y. Wang, Q. Zhang, X. Y. Li, Q. Han, M. B. Wei, Y. R. Sui, D. D. Wang, J. H. Yang, Chemical precipitation synthesis and significant enhancement in photocatalytic activity of Ce-doped ZnO nanoparticles, *Ceram. Int*., **42**, 14175 (2016).
36. M. L. Huang, Y. Yan, W. H. Feng, S. X. Weng, Z. Y. Zheng, X. Z. Fu, P. Liu, Controllable tuning various ratios of ZnO polar facets by crystal seed-assisted growth and their photocatalytic activity, *Cryst. Growth Des.*, **14**, 2179 (2014).
37. J. Duan, X. Liu, Q. Han, X. Wang, Controlled morphologies and optical properties of ZnO films and their photocatalytic activities, *J. Alloy. Compd*., **509**, 9255 (2011).
38. J. H. Zeng, B. B. Jin, Y. F. Wang, Facet enhanced photocatalytic effect with uniform single-crystalline zinc oxide nanodisks, *Chem. Phys. Lett*., **472**, 90 (2009).
39. T. Zhai, S. Xie, Y. Zhao, X. Sun, X. Lu, M. Yu, M. Xu, F. Xiao, Y. Tong, Controllable synthesis of hierarchical ZnO nanodisks for highly photocatalytic activity, *CrystEngComm*, **14**, 1850 (2012).
40. L. P. Xu, Y. L. Hu, C. Pelligra, C. H. Chen, L. Jin, H. Huang, S. Sithambaram, M. Aindow, R. Joesten, S. L. Suib, ZnO with different morphologies synthesized by solvothermal methods for enhanced photocatalytic activity, *Chem. Mater.*, **21**, 2875 (2009).
41. H. B. Lu, H. Li, L. Liao, Y. Tian, M. Shuai, J. C. Li, M. F. Hu, Q. Fu, B. P. Zhu, Low-temperature synthesis and photocatalytic properties of ZnO nanotubes by thermal oxidation of Zn nanowires, *Nanotechnology*, **19**, 338 (2008).
42. X. J. Wang, Q. L. Zhang, Q. Wan, G. Z. Dai, C. J. Zhou, B. S. Zou, Controllable ZnO architectures by ethanolamine-assisted hydrothermal reaction for enhanced photocatalytic activity, *J. Phys. Chem.* C, **115**, 2769 (2011).